

Defect-engineered ring laser harmonic frequency combs

DMITRY KAZAKOV,¹  NIKOLA OPAČAK,²  MAXIMILIAN BEISER,²  ALEXEY BELYANIN,³ 
BENEDIKT SCHWARZ,²  MARCO PICCARDO,^{1,4,*}  AND FEDERICO CAPASSO^{1,5}

¹Harvard John A. Paulson School of Engineering and Applied Sciences, Harvard University, Cambridge, Massachusetts 02138, USA

²Institute of Solid State Electronics, TU Wien, 1040 Vienna, Austria

³Department of Physics and Astronomy, Texas A&M University, College Station, Texas 77843, USA

⁴Center for Nano Science and Technology, Fondazione Istituto Italiano di Tecnologia, Milano, Italy

⁵e-mail: capasso@seas.harvard.edu

*Corresponding author: piccardo@g.harvard.edu

Received 7 May 2021; revised 11 August 2021; accepted 12 August 2021 (Doc. ID 430896); published 30 September 2021

A monochromatic wave that circulates in a nonlinear and dispersive optical cavity can become unstable and form a structured waveform. This phenomenon, known as modulation instability, was encountered in fiber lasers, optically pumped Kerr microresonators and, most recently, in monolithic ring quantum cascade lasers (QCLs). In ring QCLs, the instability led to generation of fundamental frequency combs—optical fields that repeat themselves once per cavity round trip. Here we show that the same instability may also result in self-starting harmonic frequency combs—waveforms that repeat themselves multiple times per round trip, akin to perfect soliton crystals in ring Kerr microresonators. We can tailor the intermode spacing of harmonic frequency combs by placing two minute defects with a well-defined separation between them along the ring waveguide. On-demand excitation of frequency comb states with few powerful modes spaced by hundreds of gigahertz may find their use in future sub-terahertz generators.

Published by The Optical Society under the terms of the [Creative Commons Attribution 4.0 License](https://creativecommons.org/licenses/by/4.0/). Further distribution of this work must maintain attribution to the author(s) and the published article's title, journal citation, and DOI.

<https://doi.org/10.1364/OPTICA.430896>

In passive resonators with large bulk Kerr nonlinearity, generation of multimode states results from the destabilization of an externally injected monochromatic field [1,2]. Quantum cascade lasers (QCLs), in contrast, are based on active resonators, where the optical pump is generated directly inside the cavity by electrical driving. In conventional Fabry–Perot QCLs, a multimode instability results from the nonuniform gain distribution caused by a standing-wave laser field—a phenomenon known as spatial hole burning (SHB). The frequency comb is formed when the growing side modes become frequency- and phase-locked due to resonant four-wave mixing [3–5]. Contrary to the widespread belief that in the absence of SHB and inhomogeneous spectral broadening the laser should maintain single-mode operation up to extreme pumping conditions [3,6], a dramatic lowering of the multimode

instability threshold was recently demonstrated in electrically pumped unidirectional ring QCLs [Fig. 1(a)] [7,8]. There the instability occurs due to the coupling of phase and amplitude fluctuations of the primary lasing mode via the linewidth enhancement factor (LEF) [7].

The instability that leads to frequency comb generation in ring QCLs is predicted by the complex Ginzburg–Landau equation (CGLE) where the two parameters c_D (dispersive) and c_{NL} (nonlinear) aggregate contributions from the laser group velocity dispersion (GVD), LEF, and Kerr coefficient. Depending on the values of c_D and c_{NL} , the laser may undergo instability or remain in a state of single-mode operation. The regions of the parameter space spanned by c_D and c_{NL} where the instability occurs are shown in Fig. 1(d). One set of the possible solutions in these regions are fundamental frequency comb states characterized by waveforms that repeat themselves once per cavity round trip [Fig. 1(b)]. Intermode spacing of such combs is set by the ring circumference and is equal to one cavity free spectral range (FSR).

Here we show that in addition to fundamental frequency comb states, another type of solution at different points of the parameter space is possible, corresponding to laser states with spectra of harmonic frequency combs with a certain number of skipped cavity modes. One such state that shows intermode spacing of three FSRs emerges from space–time domain simulations of a ring QCL [9] and is shown in Fig. 1(e). In the time domain the laser state constitutes a waveform that propagates in one direction and repeats itself three times within one cavity round trip [Fig. 1(f)]. The field intensity profile in steady state is characterized by low-contrast localized pulses on a continuous-wave (CW) background. The profile emerges as the result of a complex spatiotemporal field evolution during which localized structures appearing on top of the CW background of the pump field attract and repel each other, then split and merge before stabilizing in a steady-state pattern invariant between round trips [Fig. 1(g)]. This state is robust even in the presence of spontaneous emission noise that is added at every spatial grid point for each time step.

Experimental access to such states in electrically driven ring QCLs is limited. In such devices the only control knob is the injected current, whereas traversing arbitrary trajectories in the

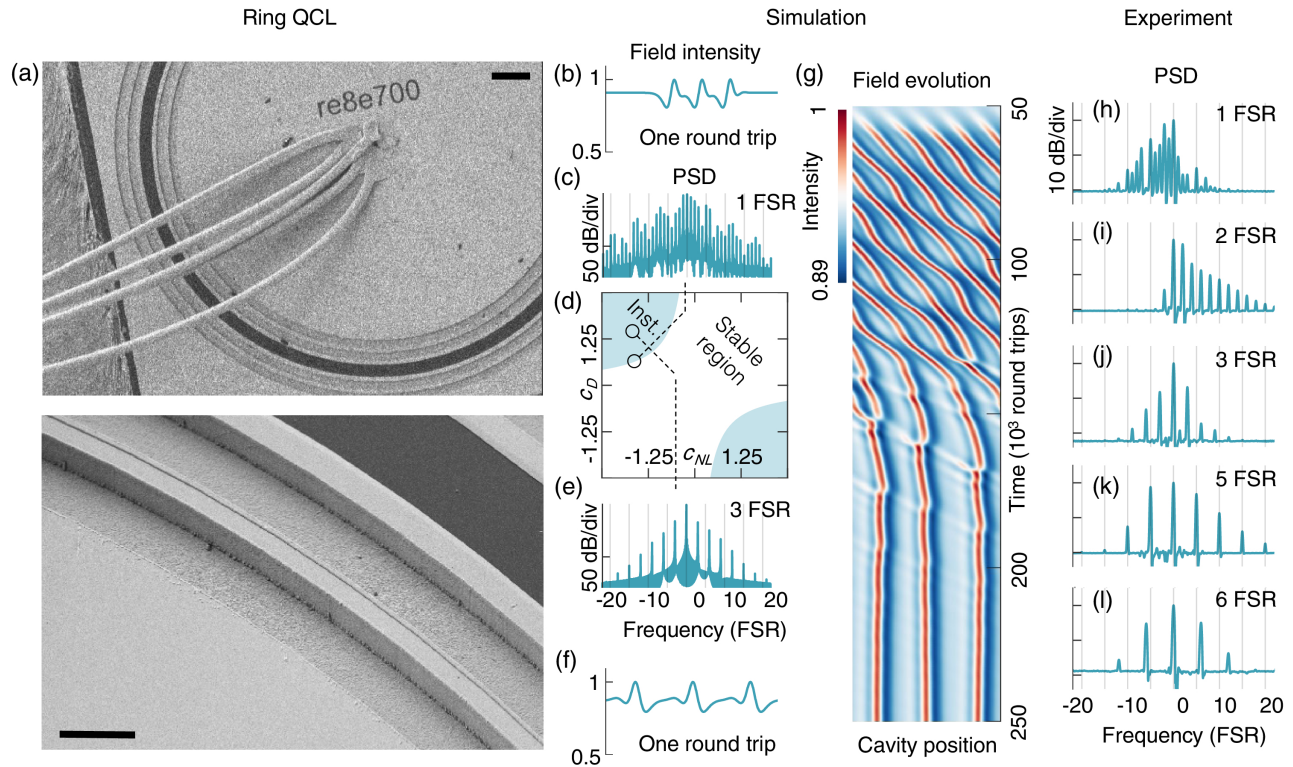


Fig. 1. (a) Scanning electron microscope image of a ring quantum cascade laser (QCL) with electrical wire bonds attached (top) and a close-up of a ring waveguide (bottom). The scale bars are 50 μm (top) and 20 μm (bottom). (b) Snapshot of the simulated steady-state field intensity of the fundamental frequency comb in the ring cavity. (c) Power spectral density (PSD) of the field in (b). All spectra are centered with respect to the dominant mode, and the frequency axis is normalized by the cavity FSR. (d) Space spanned by the parameters c_D and c_{NL} ; marked points correspond to the fundamental and harmonic comb states obtained in numerical simulations. (e) PSD of the harmonic frequency comb and (f) its steady-state field intensity in the ring cavity. (g) Simulated temporal evolution of the intracavity optical field at the onset of instability, where the final field intensity pattern corresponds to the one shown in (f). The horizontal axis is an unwrapped ring cavity angular coordinate from 0 to 2π . (h)–(l) Experimental PSD of frequency combs recorded from two ideal ring QCLs. One-FSR, two-FSR, three-FSR and five-FSR spectra are from the same device at different values of pump current; the six-FSR spectrum is from another device. FSR here is 27.8 GHz, and all lasers operate around center wavelength of 7.9 μm . Enough light escapes from the cavity via tunneling through the curved waveguide wall, which allows experimental acquisition of spectra (Supplement 1, Fig. S4).

parameter space requires independent control of the c_D and c_{NL} parameters, both dependent on the laser current. Nevertheless, we observe spontaneous generation of harmonic frequency comb states with a varying number of skipped modes both in different devices and in the same device at different injection current levels [Figs. 1(h)–1(l)]. The observation is important in that it shows that ring QCLs can generate self-starting harmonic frequency combs as the simulations predict. In such setting the states cannot be generated on demand due to the extreme sensitivity of the final comb state to the possible variations in the parameters, such as GVD and LEF, of otherwise nominally identical devices and their dependence on the driving conditions.

We propose a method that alleviates the influence of device fabrication and operation uncertainties on the attained frequency comb states and allows us to set the number of skipped modes. The method stems from the spatial dependence of the intermode beat intensity along the cavity [Fig. 2(d)], originating from the pairwise interference of any combination of lasing frequency comb modes [10]. In a unidirectional ring laser, the intensity of all intermode beat orders is constant with the angular coordinate [Fig. 2(a)]. Introducing a defect in a ring waveguide that induces a reflection and makes wave propagation bidirectional (Supplement 1, Fig. S4) leads to a change in the spatial beat profiles. They form standing waves with a number of nodes that is twice the beat order and one

of the antinodes pinned at the location of the defect [Fig. 2(b)]. To control mode skipping it is then sufficient to suppress the undesired beat orders by placing a second defect at a location of another antinode of the beat order pattern to be retained [Fig. 2(c)]. In such modified ring cavity with two defects, optical modes that get suppressed are those whose beat profiles violate the boundary conditions set by the two defects. The lowest-order beat pattern that satisfies the boundary conditions set by the defects with an angular separation of $2\pi/N$ will be N for odd N and $N/2$ for even N . We illustrate the effect of the defects on the attained comb states by comparing the spectrograms of the evolution of the laser field in a ring cavity without defects and a cavity with two defects spaced by an angle of $2\pi/5$. In ring QCL without defects, we observe at the onset of the instability a five-FSR-spaced state, which is unstable and spontaneously evolves into a three-FSR-spaced state [Figs. 2(f)–2(h)]. Adding two defects in the cavity restricts the laser only to states in which the boundary conditions set by the defects are satisfied: the laser starts in a five-FSR-spaced state at the onset of the instability, which persists all the way until the steady state is reached [Figs. 2(i)–2(k)].

We implement defects by etching narrow rectangular air slits in a ring waveguide with reflectivities between 0.4 and 0.55 [Fig. 2(e) and Supplement 1]. Here we exemplify this approach on several rings with defects that were placed using optical lithography. While

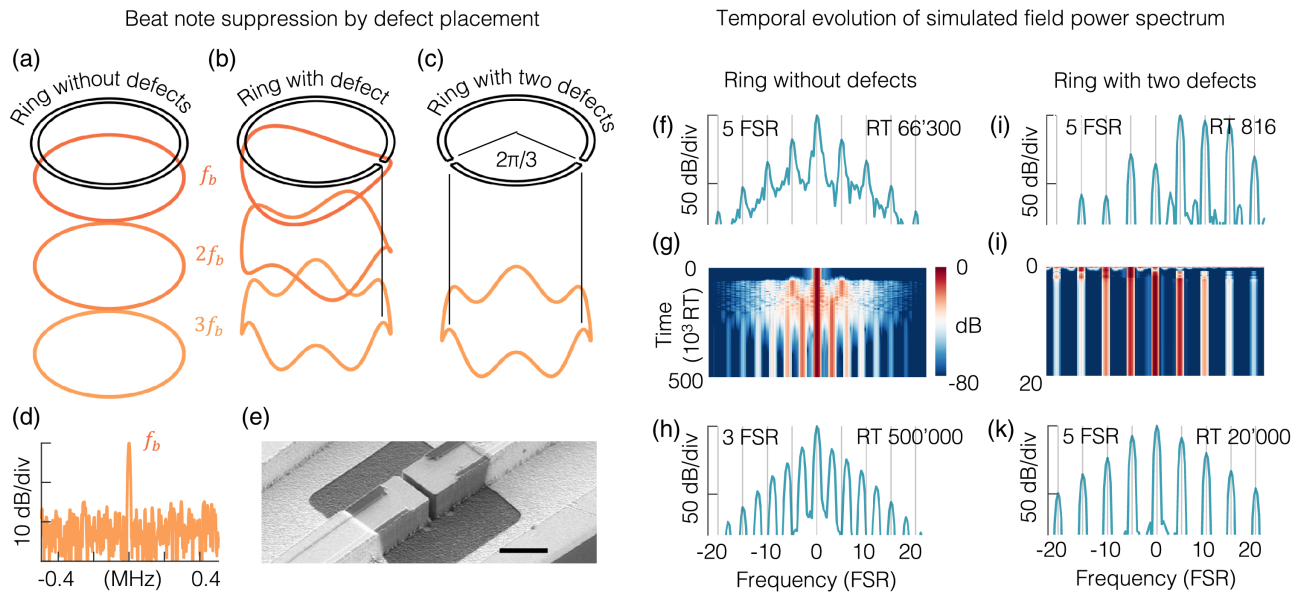


Fig. 2. (a) Spatially uniform patterns of intermode beat intensities at f_B , $2f_B$, and $3f_B$ in ring cavity without defects. (b) Profiles of intermode beatings of same orders as in (a) in a ring cavity with a single defect. The defect implemented as a subwavelength air slit in a ring waveguide pins the maximum in each of the patterns. (c) Profile of intermode beat order at $3f_B$ supported in a cavity with two defects with an angular separation of $2\pi/3$. The intermode beats at f_B and $2f_B$ are suppressed as they violate the boundary conditions imposed by the two defects. (d) Radiofrequency spectrum of an intermode beat note at f_B arising as a modulation of an electrical current and recorded by placing an RF probe on top of the ring waveguide. (e) Scanning electron microscope micrograph of a ring waveguide area with a metallization (dark gray) and passivation layer (light gray) opening and an etched slit—the defect. The waveguide width and scale bar are $10\ \mu\text{m}$. (f) Power spectral density (PSD) of the laser state in an ideal ring cavity shortly after the onset of the instability, featuring dominant peaks spaced by five FSR. RT, round trip. (g) Spectrogram of the temporal evolution of a ring QCL without defect starting from single-mode operation. The spectrogram corresponds to the spatiotemporal evolution shown in Fig. 1(g). (h) PSD of the final steady state three-FSR harmonic frequency comb in a ring cavity without defects after 500,000 round trips. (i) PSD of the laser state in a defect-engineered ring cavity with two defects spaced by $2\pi/5$ shortly after the onset of the instability, featuring dominant peaks spaced by five FSRs. (j) Spectrogram of the simulated temporal evolution of a defect-engineered ring with a defect spacing of $2\pi/5$. The five-FSR state always prevails. (k) PSD of the final steady state five-FSR harmonic frequency comb in the defect-engineered ring cavity after 40,000 round trips.

introducing a single defect in the ring waveguide promotes generation of a fundamental frequency comb with an intermode spacing of f_b [Figs. 2(d) and 3(a)], rings with two or several defects with angular separations ranging from $2\pi/5$ to $2\pi/9$ rad in different devices generate harmonic frequency combs with the corresponding number of skipped modes [Figs. 3(b)–3(e)]. Contrary to fragile harmonic frequency combs in Fabry–Perot QCLs that are highly susceptible to optical feedback and laser drive history [3], the states in defect-engineered rings are robust and are perfectly repeatable upon cycling of the laser drive current. Another advantage of the ring cavity over a Fabry–Perot cavity is the reduced optical loss that yields lasers with lower threshold, higher operating range, and larger intracavity optical power (Supplement 1, Fig. S2). Defect-engineered ring QCLs can be seen as consisting of two optically coupled cavities. In cleaved-coupled-cavity (C^3) semiconductor lasers [11], etching a gap in a Fabry–Perot cavity defines a second short section that leads to otherwise unnatural suppression of multimode lasing. In ring QCLs, on the contrary, precise defect placement favors operation in one state out of many that are inherently natural for the laser in absence of the defects.

The ring QCLs presented here are free-running with injected electrical current being the only active control knob. As a result, the range of deterministically achievable frequency comb states is either restricted by defect placement or completely absent in ring cavities without the defects, where the state generation has a stochastic nature. For applications that require readjustable intermode spacing, adding an optical coupling structure through

which the laser can be pumped optically from the outside will allow us to predictably excite reconfigurable harmonic comb states in one ring QCL with an unstructured waveguide [12,13], similarly to how it is done in microresonator Kerr combs [14]. At the same time, the geometric approach to enforce frequency comb states with predefined spacing is not restricted to QCLs and can potentially simplify generation of perfect soliton crystals (PSCs) in microresonator Kerr combs [15,16]. A modified Kerr cavity should enforce generation of PSCs with prescribed periodicity—a possibility otherwise impeded by the necessity to traverse complex trajectories in the pump parameter space. Exact physical implementation of reflective defects is not restricted to transverse air slits in a waveguide, which may induce prohibitively large diffractive losses in a high-Q microcavity: instead one can use low-contrast sidewall modulation as a defect [17]. Furthermore, our geometric approach to harmonic frequency comb generation can be used for harmonic mode locking in semiconductor lasers based on quantum well [18], quantum dash [19], and quantum dot [20] active media. An ability to engineer harmonic frequency combs in QCLs lays the foundation for future applications exploiting these sub-terahertz-spaced states with a few powerful modes that are expected to generate strong intracavity beatings [21–25]. Finally, it establishes a system with controlled settings for studying PSCs in active media strengthening the link between QCL and Kerr combs.

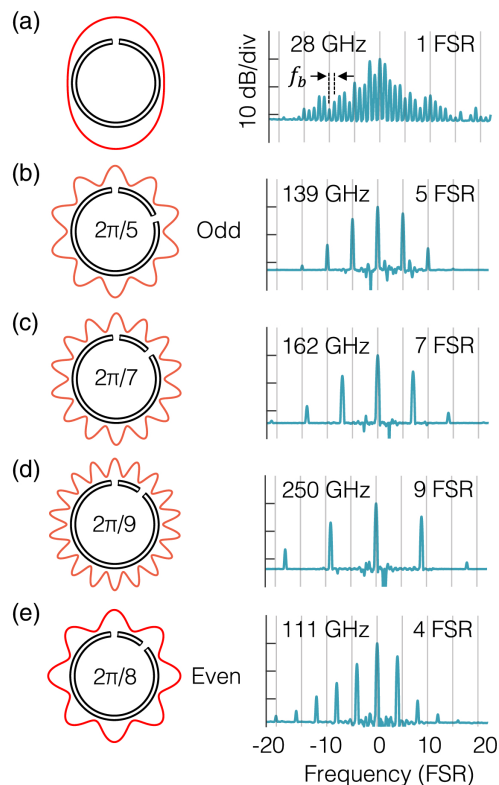


Fig. 3. (a)–(e) Mode skipping control in ring QCLs by defect engineering. Each of the panels shows a schematic of the ring waveguide with the defect arrangement, together with an overlaid polar plot showing the spatial dependence of the lowest-order intracavity beat profile selected by the defect geometry (orange line). The experimental spectrum measured from the corresponding laser is shown alongside, reporting the comb spacing in FSR units and in gigahertz. In all cases, the two defects are placed at an angle of $2\pi/N$, where N is an integer. The gray grid in the spectral plots has a spacing of five FSRs.

Funding. European Research Council (ERC) (853014); Austrian Science Fund (FWF) (NanoPlas); National Science Foundation (1541959, CCSS-1807323).

Acknowledgment. Any opinions, findings, conclusions, or recommendations expressed in this material are those of the authors and do not necessarily reflect the views of the National Science Foundation. B. Schwarz was supported by the FWF within the project NanoPlas and by the ERC under the European Union's Horizon 2020 research and innovation program.

Disclosures. The authors declare no conflicts of interest.

Data availability. Data underlying the results presented in this paper are not publicly available at this time but may be obtained from the authors upon reasonable request.

Supplemental document. See Supplement 1 for supporting content.

REFERENCES

1. T. J. Kippenberg, R. Holzwarth, and S. A. Diddams, *Science* **332**, 555 (2011).
2. T. J. Kippenberg, A. L. Gaeta, M. Lipson, and M. L. Gorodetsky, *Science* **361**, eaan8083 (2018).
3. T. S. Mansuripur, C. Vernet, P. Chevalier, G. Aoust, B. Schwarz, F. Xie, C. Caneau, K. Lascola, C.-E. Zah, D. P. Caffey, T. Day, L. J. Missaggia, M. K. Connors, C. A. Wang, A. Belyanin, and F. Capasso, *Phys. Rev. A* **94**, 063807 (2016).
4. Y. Wang and A. Belyanin, *Phys. Rev. A* **102**, 013519 (2020).
5. D. Burghoff, *Optica* **7**, 1781 (2020).
6. H. Risken and K. Nummedal, *J. Appl. Phys.* **39**, 4662 (1968).
7. M. Piccardo, B. Schwarz, D. Kazakov, M. Beiser, N. Opačak, Y. Wang, S. Jha, J. Hillbrand, M. Tamagnone, W. T. Chen, and A. Y. Zhu, *Nature* **582**, 360 (2020).
8. B. Meng, M. Singleton, M. Shahmohammadi, F. Kapsalidis, R. Wang, M. Beck, and J. Faist, *Optica* **7**, 162 (2020).
9. N. Opačak and B. Schwarz, *Phys. Rev. Lett.* **123**, 243902 (2019).
10. M. Piccardo, D. Kazakov, N. A. Rubin, P. Chevalier, Y. Wang, F. Xie, K. Lascola, A. Belyanin, and F. Capasso, *Optica* **5**, 475 (2018).
11. W. T. Tsang, N. A. Olsson, and R. A. Logan, *Appl. Phys. Lett.* **42**, 650 (1983).
12. F. Prati, M. Brambilla, M. Piccardo, L. L. Colombo, C. Silvestri, M. Gioannini, A. Gatti, L. A. Lugiato, and F. Capasso, in *Frontiers in Optics and Photonics 1* (De Gruyter, 2021), p. 197.
13. L. Colombo, M. Piccardo, F. Prati, L. Lugiato, M. Brambilla, A. Gatti, C. Silvestri, M. Gioannini, N. Opačak, B. Schwarz, and F. Capasso, *Phys. Rev. Lett.* **126**, 173903 (2021).
14. D. C. Cole, E. S. Lamb, P. Del'Haye, S. A. Diddams, and S. B. Papp, *Nat. Photonics* **11**, 671 (2017).
15. M. Karpov, M. H. Pfeiffer, H. Guo, W. Weng, J. Liu, and T. J. Kippenberg, *Nat. Phys.* **15**, 1071 (2019).
16. J. K. Jang, X. Ji, C. Joshi, Y. Okawachi, M. Lipson, and A. L. Gaeta, *Phys. Rev. Lett.* **123**, 153901 (2019).
17. S.-P. Yu, D. C. Cole, H. Jung, G. T. Moille, K. Srinivasan, and S. B. Papp, *Nat. Photonics* **15**, 461 (2021).
18. S. Arahira, Y. Matsui, and Y. Ogawa, *IEEE J. Quantum Electron.* **32**, 1211 (1996).
19. G. Liu, Z. Lu, J. Liu, Y. Mao, M. Vachon, C. Song, P. Barrios, and P. J. Poole, *Opt. Express* **28**, 4587 (2020).
20. D. Auth, V. Korenev, A. Savelyev, M. Maximov, A. Zhukov, and S. Breuer, *J. Phys. Conf. Ser.* **1695**, 012068 (2020).
21. T. E. Drake, T. C. Briles, J. R. Stone, D. T. Spencer, D. R. Carlson, D. D. Hickstein, Q. Li, D. Westly, K. Srinivasan, S. A. Diddams, and S. B. Papp, *Phys. Rev. X* **9**, 031023 (2019).
22. S.-W. Huang, J. Yang, S.-H. Yang, M. Yu, D.-L. Kwong, T. Zhevinsky, M. Jarrahi, and C. W. Wong, *Phys. Rev. X* **7**, 041002 (2017).
23. V. Pistore, H. Nong, P.-B. Vigneron, K. Garrasi, S. Houver, L. Li, A. G. Davies, E. H. Linfield, J. Tignon, J. Mangeney, R. Colombelli, M. S. Vitiello, and S. S. Dhillon, *Nat. Commun.* **12**, 1427 (2021).
24. T. Nagatsuma, G. Ducournau, and C. C. Renaud, *Nat. Photonics* **10**, 371 (2016).
25. M. Piccardo, M. Tamagnone, B. Schwarz, P. Chevalier, N. A. Rubin, Y. Wang, C. A. Wang, M. K. Connors, D. McNulty, A. Belyanin, and F. Capasso, *Proc. Natl. Acad. Sci. USA* **116**, 9181 (2019).